Available online at www.sciencedirect.com
SCIENCE DIRECT
Journal of Power Sources 158 (2006) 45–51
JOURNAL OF POWER SOURCES
www.elsevier.com/locate/jpowsour

Interpretation of the interconnected microstructure of an NiO-YSZ anode composite for solid oxide fuel cells via impedance spectroscopy

K.-R. Lee [a], Y.S. Pyo [b], B.S. So [b], S.M. Kim [b], B.K. Lee [b], J.H. Hwang [b,*], J. Kim [a], J.-H. Lee [a], H.-W. Lee [a]

[a] *Nano-Materials Research Center, Korea Institute of Science and Technology, Seoul 136-791, Republic of Korea*
[b] *Department of Materials Science and Engineering, Hongik University, Sangsu-dong, Mapo-gu, Seoul 121-791, Republic of Korea*

Received 1 June 2005; accepted 1 September 2005
Available online 19 October 2005

Abstract

Impedance spectroscopy is applied to characterize the porous microstructure of NiO-YSZ composites for solid oxide fuel cells after the pores are filled with a highly conductive aqueous medium. The apparent electrical characteristics are combined with conventional electrocomposite theory to describe the whole system, namely, a high resistivity component of an NiO-YSZ composite phase and a low resistivity component of a liquid phase, infiltrating the pores of the NiO-YSZ system. The resultant electrical information is probably due to the ionic conduction through the liquid phase within the pores of the NiO-YSZ composites. Image analysis is applied in order to characterize the microstructure of the NiO-YSZ composites. Furthermore, to determine the interconnectivity of the pores in the NiO-YSZ composite, which is a key microstructural factor, the microstructural information is combined with the electrical characteristics obtained through impedance spectroscopy. The interconnectivity of the pores is found to be lower than that estimated from two-dimensional image analysis.

Keywords: Solid oxide fuel cell; Image analysis; Impedance spectroscopy; Interconnectivity; Nickel oxide and yttria-stabilized zirconia composite

1. Introduction

A solid oxide fuel cell (SOFC) is an efficient high-temperature energy conversion system in which a gaseous fuel and an oxidizing gas are combined electrochemically to generate electricity and heat. Furthermore, the SOFC produces negligible amounts of SO_x and NO_x, and thereby protects the environment from fossil-based pollution such as acid rain and photochemical smog. SOFCs can be applied to stationary and residential power, transportation, portable power, landfills or waster treatments, and so on. These advantages have highlighted the value of SOFCs in energy-related and environment-related industries. Until now, however, most research has focused on the synthesis and processing of materials, along with cell fabrication and subsequent operational tests [1–3].

The key components of SOFCs are electrolytes, anodes and cathodes. Of these components, anodes are crucial for providing the reaction sites for the electrochemical oxidation of fuel. Moreover, in the case of anode-supported cells, anodes provide mechanical support for thin-film electrolytes and a path for supplying fuel to reaction sites. The most promising anode materials in terms of electrochemical activity and cost are cermet compounds of Ni and yttria-stabilized zirconia (YSZ).

For the best performance of SOFC anodes, it is most important to ensure that the anode microstructure minimizes the polarization loss at the anode during operation. There are two major sources of this polarization loss, namely: (i) activation polarization loss, which is mostly related to the low electrochemical activity of the anode; (ii) diffusional or concentration polarization loss, which is due to an insufficient supply of reactants to the reaction site of the anode. These types of polarization loss strongly depend on the microstructural factors of the anode, such as size, spatial distribution and the interconnectivity of each constituent phase. In particular, diffusional polarization loss is closely related to the pore structure of the anode, especially the connectivity of the pores within the microstructure.

Previously, we reported [4,5] that the initial microstructure of the NiO-YSZ composite determines the ultimate porous features

* Corresponding author. Tel.: +82 2 320 3069; fax: +82 2 333 0127.
E-mail address: jhwang@wow.hongik.ac.kr (J.H. Hwang).

0378-7753/$ – see front matter © 2005 Elsevier B.V. All rights reserved.
doi:10.1016/j.jpowsour.2005.09.011

of Ni-YSZ anode cermets, and that the porous features consequently affect the final performance of SOFCs [4,5]. Despite the potential significance of the microstructural features of anode composites, rare microstructural characterizations of the interconnected pores have been reported for Ni-YSZ anodes. As yet, neither the microstructural features nor the operational mechanisms of the anode are completely understood, though the proper electrochemical reactions at the anode and electrolyte are widely accepted as essential for the optimum operation of SOFCs.

Impedance spectroscopy is a highly powerful tool for investigating the electrical properties in electrocomposites such as SOFC electrodes, grain boundary–controlled ceramics, and cementitious materials [6–10]. In general, impedance spectroscopy can effectively separate electrode-related effects from bulk properties by differentiating the time constants of each conduction process; that is, the grain interiors, the grain boundaries, and the electrode-related responses. Impedance spectroscopy can also provide information on the homogeneity of the microstructural features that govern the apparent impedance response from the depression level of the bulk impedance arcs below the real axis in Nyquist plots ($-Z_{imag}$ versus Z_{real}). Moreover, after obtaining the effective dielectric constant, it is possible to determine whether the bulk response arises from the solid phase or from the interfaces.

Focus is placed on the microstructural features of the interconnected pores in the NiO-YSZ composites, and impedance spectroscopy is combined with image analysis to interpret the microstructural usefulness of these composites in terms of the effective supply of fuel gas.

2. Experimental

Electrical characterization of the NiO-YSZ composites, was conducted by means of the apparatus shown in Fig. 1, that was designed for impedance spectroscopy. The porous NiO-YSZ composites, which were filled with a dissolved solution of 5 wt.% NaCl, were boiled in an identical solution until the pores were completely filled with the NaCl-containing solution. The specimens were inserted into the measurement apparatus and thereby divided the liquid medium into two compartments. The concentration of the liquid medium in each compartment was identical to that of the solution that filled the pores of the NiO-YSZ specimens. The liquid was incorporated into the measuring apparatus to guarantee an intimate contact between the liquid medium and the NiO-YSZ composite that thereby ensures the flow of current during the impedance measurement.

The starting materials were NiO (Sumitomo, Japan), coarse YSZ (Unitec, UK) and fine YSZ (Tosoh, Japan) in a mixing ratio of 56:22:22 wt.%. The average particle sizes of the fine and coarse YSZ and the NiO were 0.25, 1.8 and 0.8 μm, respectively. After ball-milling the premixed powders in proper solvents for 12 h, the products were granulated to help compact the powder at the forming stage. A liquid condensation process was used for the granulation in which a polymer resin was employed as both a deformable fugitive phase and a binder, and thereby produced additional porosity after the heat treatment [4]. To obtain the different microstructural features of the anode substrate, granules of the NiO-YSZ mixture were compacted and uniaxially pressed, under a pressure that ranged from 7 to 28 MPa, into a pellet with a diameter of 35 mm and a thickness of approximately 1 mm. The uniaxially pressed NiO-YSZ substrates were then sintered at 1350 °C in air for 3 h.

The Archimedes method was used to measure the density of the NiO-YSZ substrates as a function of the compaction pressure. The porosity of the samples was determined with a mercury porosimeter (Micrometrics, USA), and the gas permeability was measured with a perm porometer (PMI, USA). To analyze the images, the NiO-YSZ cermet sample was prepared in accordance with a general ceramographic method. Given the porous nature of the NiO-YSZ mixture, a bare specimen can suffer from mechanical damage, which leads to misinterpretation of the microstructural analysis. Therefore, a polymer infiltration method similar to that of Simowonis et al. [11] was adopted. To avoid any microstructural damage in the NiO-YSZ cross-section, an epoxy resin was infiltrated into the NiO-YSZ composite and then cured in an electrical oven until the pore skeleton was rigidly formed. After the curing, the substance was polished with abrasive paper and diamond pastes. An optical microscope (Zeiss Axiovert, Germany) equipped with a digital camera (JVC KY-F70, Japan) and a scanning electron microscope (FEI XL-30, USA) were used to capture digital images of the NiO-YSZ electrocomposites. The images were analyzed with the commercially available software Image-Pro (Image-Pro, Media Cybernetics, USA) in conjunction with quantitative microscopic theory. This combination enabled the separation of each constituent phase (that is, the pore and the solid composite of the NiO-YSZ), as well the quantification of various microstructural parameters such as the size, distribution and contiguity of each phase.

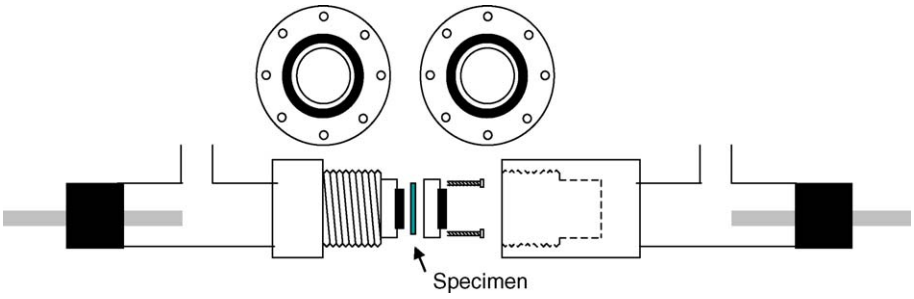

Fig. 1. Measurement apparatus for electrical characterization using impedance spectroscopy.

Studies with ac impedance spectroscopy were conducted with a HP 4192A instrument (Hewlett Packard, Palo Alto, USA) that had specially designed fixture, along with a highly conductive solution (5 wt.% NaCl in water) as the conducting medium. The measurements were taken between 5 Hz and 1 MHz at room temperature, with 10 points per decade. To eliminate stray admittance, such as fixture capacitance and electrode inductance, an open/short-circuit correction was applied. After collecting impedance spectra, the constants of the relevant materials were calculated by considering the geometric factors of each specimen.

3. Results and discussion

3.1. Image analysis

Previously, we introduced [12] a method of image analysis that was suitable for characterizing the microstructure of Ni-YSZ SOFC anodes. Based on two-dimensional microscopic information, the image analyzing approach enabled all the constituent phases of the anode materials to be differentiated. This differentiation subsequently allowed quantitative analysis of the microstructural parameters, especially the parameters related to the pore structure of the anode such as porosity and interconnectivity or contiguity.

Typical micrographs of the NiO-YSZ composite exposed to low and high compaction pressures and subsequent sintering are given in Figs. 2(a) and 3(a). The micrographs were converted into two components: (i) a solid portion made up of NiO and YSZ particles and (ii) another portion of pores in the system. The combined image was deconvoluted into the two independent binary images (shown in Figs. 2(b) and 3(b)) for analyzing the microstructure in more detail. The separated images of the solid phase (which is made up of NiO and YSZ) and the pore phase are clearly differentiated for the quantitative analysis of each constituent phase. Using these deconvoluted binary images, the line-interception method was applied to characterize the composite's microstructural parameters, such as the porosity, size, size distribution, and the contiguity of the selected phases—that is, the solid phase and the pore phase.

The detailed approach that incorporates line interception is described elsewhere [13]. By analyzing the microstructure with the line interception method, the volume fractions of the solid phase and the pore phase can be determine accurately especially by comparing image analysis and actual measurements taken with the Archimedes method and mercury porosimetry [12].

Two-dimensional information on the area fraction of the pore phase, which is equivalent to the porosity of the NiO-YSZ composite is summarized in Table 1. In addition, the pore size distributions for low and high compaction pressures are shown in Fig. 4. As expected, and as shown in Table 1, the calculated volume fraction of the pores decreases as the compaction pressure increases. Moreover, as the compaction pressure increases, the pore-size distribution becomes narrower, the average pore size decreases, and the fraction of small pore sizes increases.

Such two-dimensional microscopic information can be combined with quantitative stereographic theory to provide three-dimensional contiguity or equivalent interconnectivity [14–21]. According to quantitative stereological theory, the interconnectivity can be expressed as follows, where the β_i (image) of one specific phase is a fraction of the contact areas (S_v^i) of the corresponding phase against the total inner surface:

$$\beta_i\,(\text{image}) = \frac{S_v^i}{\sum_i S_v^i}. \tag{1}$$

The volume to surface area ratio (V_i/S_v^i) of phase i can be defined as:

$$\frac{V_i}{S_v^i} = \frac{l_i}{4}, \tag{2}$$

where l_i is the intercept length of phase i and is derived from the two-dimensional image analysis with the line-intercept concepts.

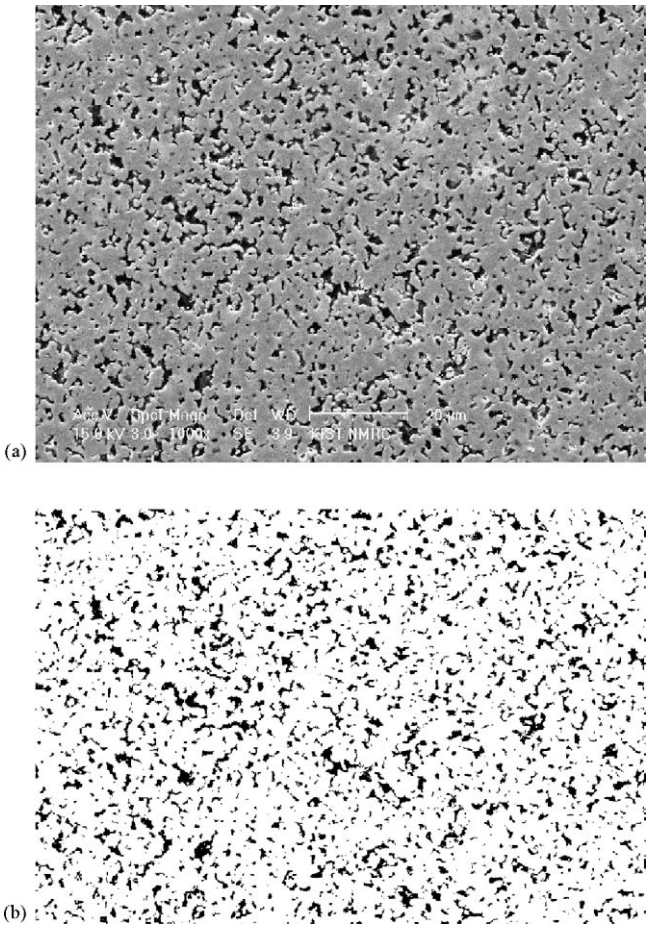

Fig. 2. Micrographs of NiO-YSZ composite compacted under 7 MPa: (a) original image and (b) deconvoluted pore-phase image.

Table 1
Porosities determined from image analysis

Compaction pressure (MPa)	Porosities (%)
7	12.02
14	9.84
21	6.85
28	6.79

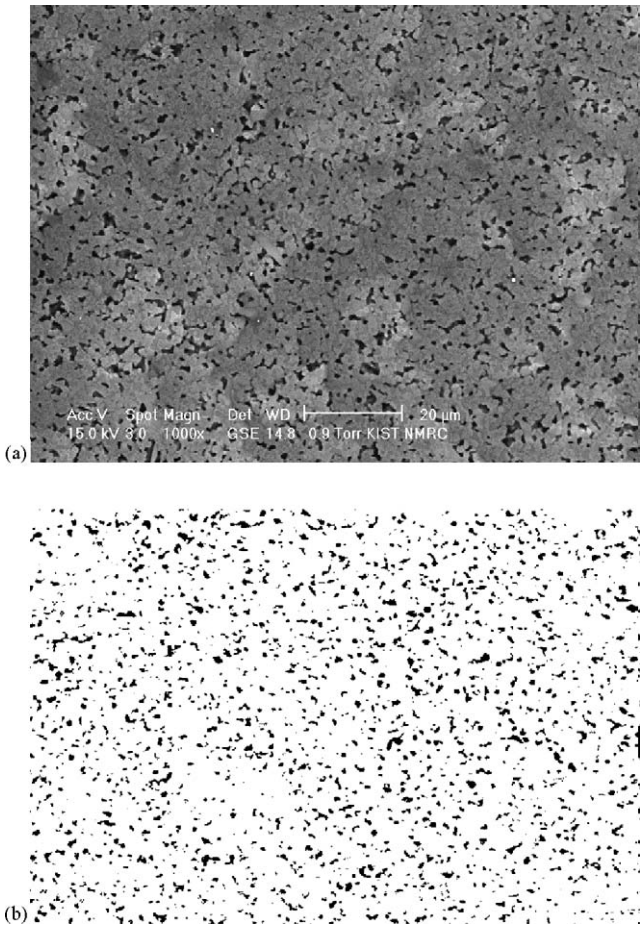

Fig. 3. Micrographs of NiO-YSZ composite compacted under 28 MPa: (a) original image and (b) deconvoluted pore-phase image.

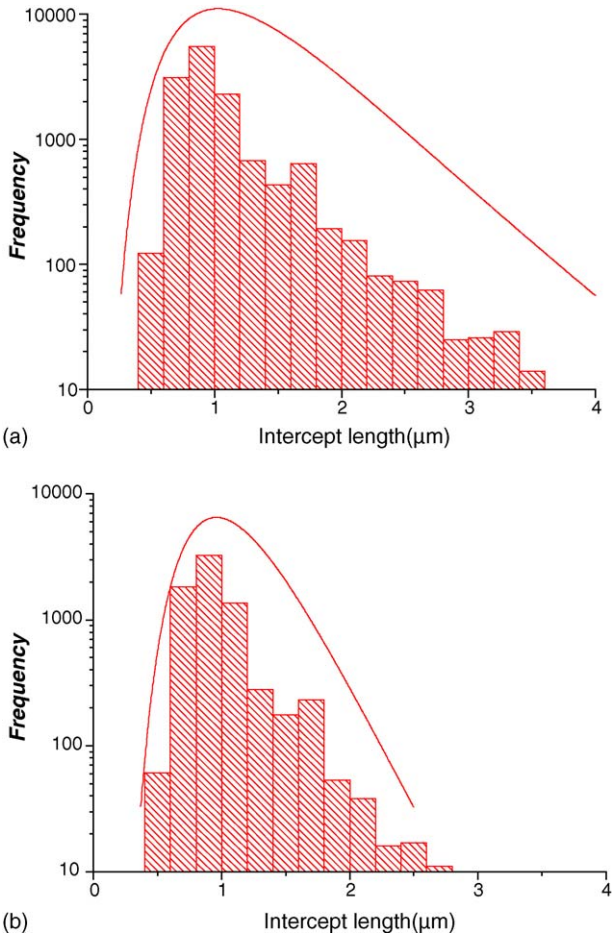

Fig. 4. Pore-size distribution of sintered NiO-YSZ composite compacted under different compaction pressures: (a) low compaction pressure (7 MPa) and (b) high compaction pressure (28 MPa).

From Eqs. (1) and (2), the three-dimensional interconnectivity of the pores, that is, the β_{pore} (image), can be expressed as follows:

$$\beta_{\text{pore}}\,(\text{image}) = \frac{V_{\text{pore}} l_{\text{solid}}}{V_{\text{pore}} l_{\text{solid}} + V_{\text{solid}} l_{\text{pore}}}. \tag{3}$$

The calculated interconnectivities from the quantitative analysis of the two-dimensional micrographs are given in Fig. 5. According to the electrocomposite theory, the interconnectivity value of 1 (one) can be obtained when all the pores between two electrodes are connected in a straight fashion (as with cylindrical pores) without any deviating paths, whereas the interconnectivity of closed pores leads to 0 (zero) because the isolated pores cannot form a continuous path. By contrast, the interconnectivity of pores, the β_{pore} (image) from image analysis with two-dimensional micrographs can be used to consider not only interconnected pores through the specimens but also the closed pores and disconnected pores at external surface. As a result, this image analyzing method can overestimate the real fraction of pores interconnected through the specimens, and thus result in a high value for the interconnectivity.

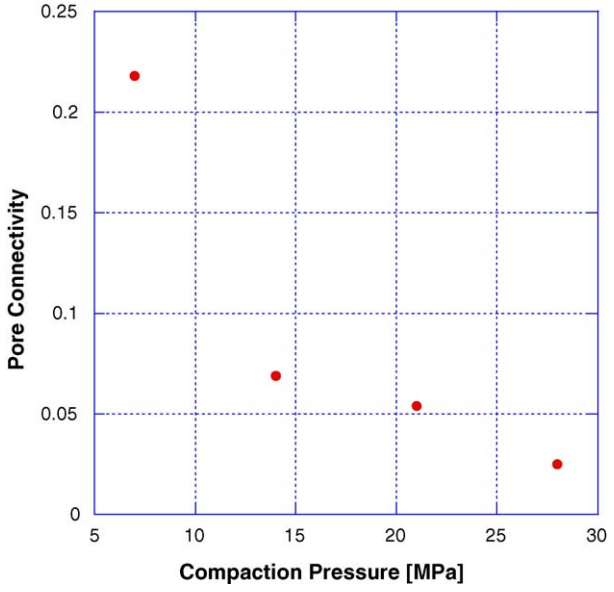

Fig. 5. Interconnectivity of pores determined from image analysis.

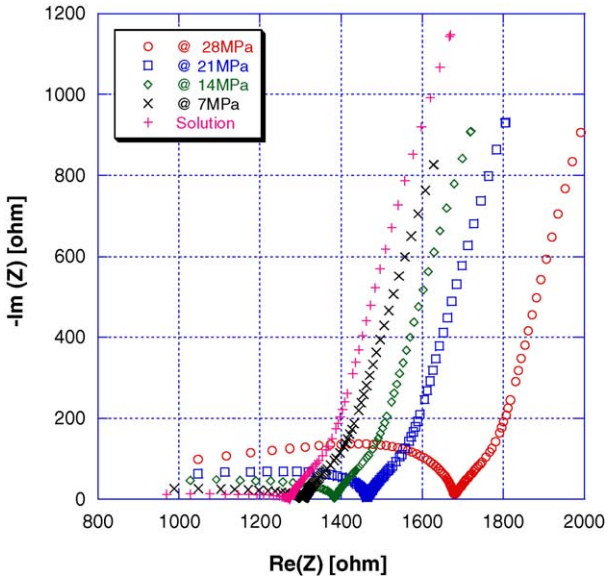

Fig. 6. Impedance spectra as a function of compaction pressure.

3.2. Impedance spectroscopy

The impedance spectra of NiO-YSZ composites are presented in Fig. 6. In each spectrum, the frequency increases from right to left. There is an incomplete depressed arc at low frequencies (the right part of the impedance spectrum) and another arc at high frequencies (the left part of the impedance spectrum). The low-frequency impedance arc is attributed to electrode polarization with a high capacitance value of 10^{-6} F at 10 Hz. The high-frequency response is found to be due to a bulk response; that is, ionic conduction in a liquid state, because the dielectric constant is approximately equal to that of the water. The high frequency arc expands as the compaction pressure is raised. Distortion of the impedance arcs should be noted, even though a correction was made for the undesired contribution of the measurement apparatus, such as stray inductive and capacitive components. In other words, the inductive component of the high conductivity medium, which still plays a role in the opposite direction to that of the capacitive component in the impedance arc, appears to depress the arcs into the real axis.

The bulk arc was modelled as a resistor (R) and as a capacitor (C) in a parallel-series arrangement or as two parallel RC circuits in series. The equivalent circuits are shown in Fig. 7. The contributions from the electrodes and the liquid (aqueous solution of NaCl) are the superimpositions of two segments on both sides of the specimen. The high-frequency part of the impedance spectra arises from a complex summation of the liquid and the NiO-YSZ composite that has numerous resistor and capacitor components.

The impedance spectra in Fig. 6 is used to calculate the magnitude of the impedance and capacitance (see Fig. 8). In this study, the bulk resistance is calculated from the inflection point that touches the real axis. The bulk resistance, which occurs in high-frequency regimes, is determined by simply adding the resistance from the liquid portion to the resistance of the composite whose pores are filled with the NaCl-containing solution. These characteristics, which enable separation of the electrical information from the electrocomposites, can be used the subsequent microstructural analysis.

Noticeably, the capacitance increases as the compaction pressure increases, that is, as the average pores size decreases, while a narrow distribution of pores simultaneously concurs with increase in the portion of disconnected pore paths. In addition, the calculated dielectric constant is higher than that of either the solid phase or the liquid medium, this indicates that a dielectric amplification occurs in the porous medium which is filled with a highly conductive liquid (see Fig. 8). Similar phenomena have been reported for cement-based materials [22]. The present system does not, however involve the products obtained from the reactants as a function of time.

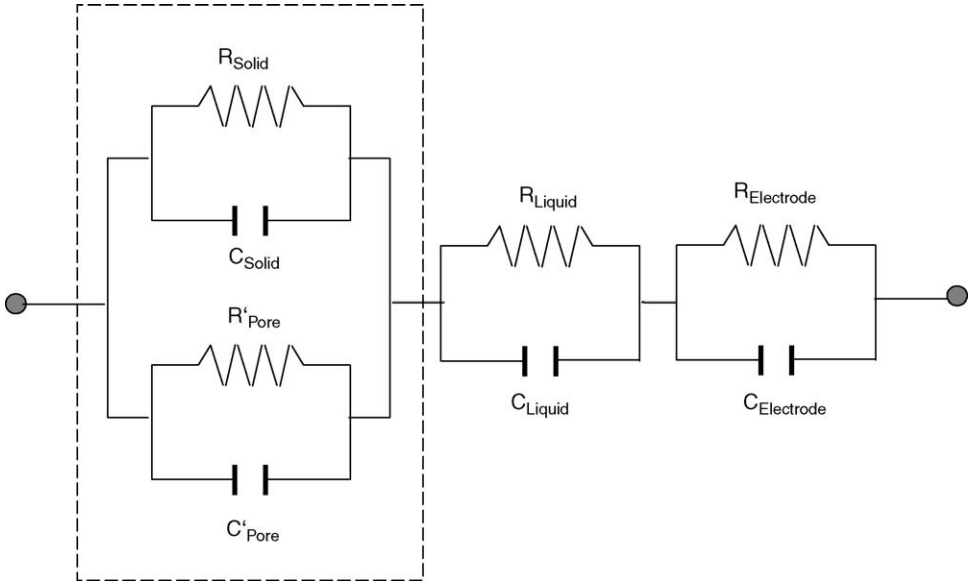

Fig. 7. Equivalent circuit representing NiO-YSZ electrocomposite with high conductive liquid in pores.

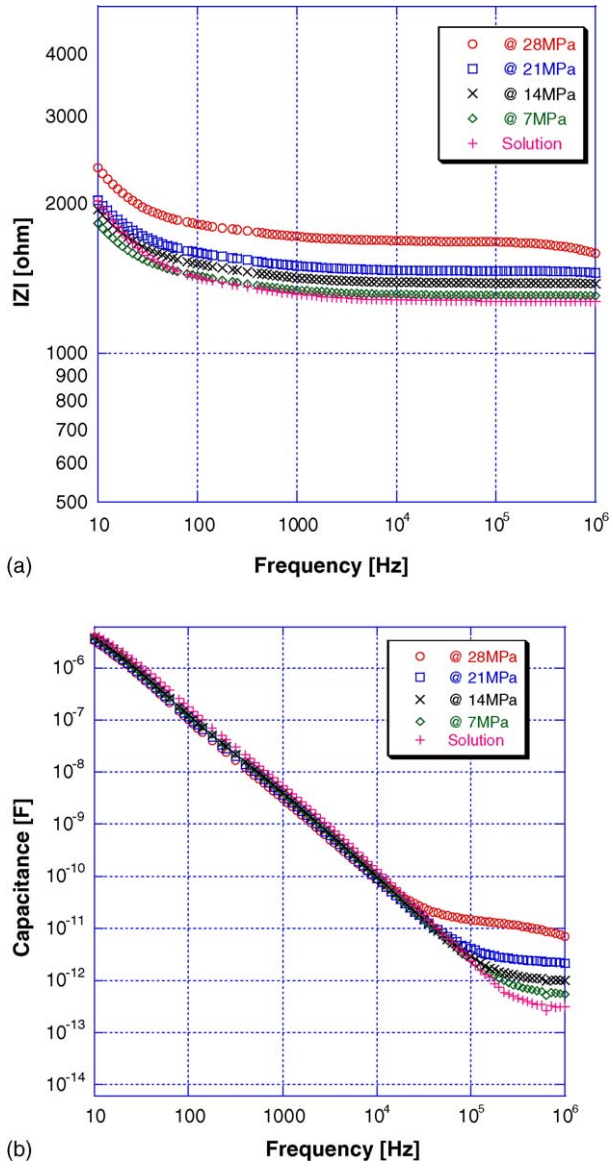

Fig. 8. Capacitance vs. frequency as a function of compaction pressure.

To understand the dielectric behavior, the way in which the pore size affects the dielectric capacitance was simulated. The measured capacitance was found to be related inversely to the size of the pores. In the simulation experiment, the dielectric response resembles a structure constructed from plates with holes. The capacitance of the slab-like solid phase, which is separated with water, is believed to dominate the capacitance values, and causes dielectric amplification when the equivalent dielectric constants are higher than the values of the constituent phases.

The capacitances obtained suggest that, in line with the electrocomposite theory, the electrical properties of the NiO-YSZ composite are dominated by the ionic solution in the pore network. The bulk resistivity of the NiO-YSZ composite is therefore discussed in terms of electrocomposite concepts [23]. The present system is made up of two phases, a solid phase and a pore phase. The solid phase is a composite of NiO and YSZ. The connectivity of the solid and pore phases are 3-3, where the numbers represent the NiO-YSZ composite (connected in 3D) and the pore phase (also connected in 3D). The overall conductivity, σ_t, is approximated as

$$\sigma_t = \sum \sigma_i \phi_i \beta_i = \sigma_s \phi_s \beta_s + \sigma_l \phi_l \beta_l \quad (4)$$

where σ_i is the phase conductivity, ϕ_i is the volume fraction of the phase, and β_i is the connectivity parameter with the interconnectivity ranging between 0 and 1 (the solid phase is denoted by s and the liquid denoted by l). Given the anticipated extremely low conductivity of NiO and YSZ, the solid phase makes little or no contribution. By contrast, the deionized water with the dissolved sodium chloride shows a very high value of conductivity, that is, 0.092 $(\Omega\,\mathrm{cm})^{-1}$ at room temperature. Taking into account the conductivity contribution, the above equation can be simplified as follows:

$$\sigma_t \approx \sigma_l \phi_l \beta_l \quad (5)$$

where the interconnectivity, β_l, is a measure of the connectivity (or inversely of the tortuosity) of the pore phase.

The conductivity of the liquid phase via the pore phase and the pore fraction of the constituent phase should be determined in advance in order to calculate the interconnectivity in the porous structure. In this study, the conductivity of the pure liquid phase and the NiO-YSZ composites that were infiltrated with the high conductivity phase were measured in accordance with the experimental set-up described above in the experimental section. Furthermore, in the previous image analysis, the pore fraction, or porosity, was also characterized successfully with the aid of line-intercept concepts. From all these results, the calculated interconnectivity values from Eq. (5) are plotted in Fig. 9, along with the information obtained from the image analysis. As shown in Fig. 9, the interconnectivity from the impedance work is lower than that from the image analysis techniques. The difference ranges from 0.14 to 0.29 (in an absolute scale where the

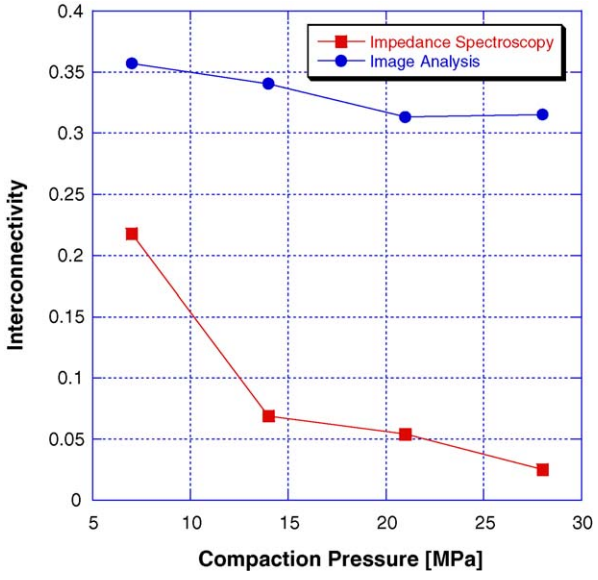

Fig. 9. Comparison of interconnectivity of pores obtained via impedance spectroscopy and image analysis.

maximum value is 1), and the deviation becomes larger as the compaction pressure increases. The huge difference between the two results strongly suggests that the pore paths between the two electrodes are not straightforward, i.e. it is expected that there is high tortuosity and that the many pore paths from the specimen surface exposed to the electrodes are disconnected so that the portion of pore paths disconnected is not considered sufficiently in the impedance work. The interconnectivity is therefore lower than that obtained from image analysis.

It may be concluded that the prediction of pore interconnectivity through image analysis can limit the practical estimation of interconnected pores across the composites as the porosity decreases. This is because the analysis is based on a smaller number of micrographs obtained from limited portions of the polished surface of the composites. By contrast, the impedance approach, which reflects the information collected across the entire specimen, provides a more accurate estimate of the interconnectivity. It is therefore concluded that image analysis can normally give the highest limit on interconnectivity while the impedance work supports the experimental estimation in a more realistic manner.

Nonetheless, in this study, the effectiveness of impedance spectroscopy can be verified by using the information on the volume fraction of the constituent phases (solid and pore). In conjunction with image analysis, impedance spectroscopy can be standardized in upcoming research and development, particularly for the purpose of evaluating electrode precursors for SOFCs, that is, NiO-YSZ or any equivalent anode precursors.

4. Conclusion

Image analysis has been combined with impedance spectroscopy to understand the microstructure of the electrocomposite NiO-YSZ, which is a precursor for the anodes of SOFCs. Using stereographic quantitative analysis of two-dimensional micrographs, image analysis has been used to calculate the porosity and interconnectivity. Furthermore, impedance spectroscopy has been employed to estimate the interconnectivity as a function of the compaction pressure, while considering the concept of ionic conduction of liquid phase that infiltrates the porous structure of the NiO/YSZ. In both image analysis and impedance spectroscopy, it is found that interconnectivity decreases as the compaction pressure increases. Nevertheless, the interconnectivity detected by impedance spectroscopy is lower than that by image analysis. At the highest compaction pressure, the difference is more than 20%, which indicates that the three-dimensional complexity is reflected effectively by impedance spectroscopy. This is because the technique uses direct measurement of the entirety of each specimen rather than estimates based on the two-dimensional surfaces in image analysis.

Acknowledgements

The authors are supported by the Core Technology Development Program for Fuel Cells, under the aegis of the Ministry of Science and Technology in the Republic of Korea.

References

[1] B.C.H. Steele, A. Heinzel, Nature 414 (2001) 345.
[2] J.M. Ralph, A.C. Schoeler, M. Krumpelt, 36 (2001) 1161.
[3] C. Xia, F. Chen, M. Liu, Electrochem. Solid State Lett. 4 (5) (2001) A52.
[4] D.-S. Lee, J.-H. Lee, J. Kim, H.-W. Lee, H.S. Song, Solid State Ionics 166 (2004) 13.
[5] J.-H. Lee, J.-W. Heo, D.-S. Lee, J. Kim, G.-H. Kim, H.-W. Lee, H.S. Song, J.-H. Moon, Solid State Ionics 158 (2003) 225.
[6] J.E. Baurele, J. Phys. Chem. Solids 30 (1969) 2657.
[7] J.T.S. Irvine, D.C. Sinclair, A.R. West, Adv. Mater. 2 (3) (1993) 132.
[8] I.M. Hodge, M.D. Ingram, A.R. West, J. Electroanal. Chem. 74 (1976) 125.
[9] D.C. Sinclar, A.R. West, J. Appl. Phys. 66 (8) (1989) 3850.
[10] B.J. Christensen, R.T. Coverdale, R.A. Olson, S.J. Ford, E.J. Garboczi, H.M. Jennings, T.O. Mason, J. Am. Ceram. Soc. 77 (1994) 2789.
[11] D. Simwonis, F. Tietz, D. Stoever, Solid State Ionics 132 (2000) 241.
[12] K.-R. Lee, S.H. Choi, J. Kim, H.-W. Lee, J.-H. Lee, J. Power Sources 140 (2005) 226.
[13] J.H. Lee, H. Moon, H.-W. Lee, J. Kim, J.-D. Kim, K.-H. Yoon, Solid State Ionics 148 (2002) 15.
[14] J. Gurland, Trans. Metall. Soc. AIME 212 (1958) 452.
[15] J. Gurland, Trans. Metall. Soc. AIME 236 (1966) 642.
[16] Z. Fan, Philos Magn. A 72 (1996) 1663.
[17] Z. Fan, A.P. Miodownik, P. Tsakiropoulos, Mater. Sci. Technol. 9 (1993) 1094.
[18] K.B. Alexander, P.F. Becher, S.B. Waters, A. Bleiter, J. Am. Ceram. Soc. 77 (4) (1994) 939.
[19] E.E. Underwood, Stereologia 3 (1964) 5.
[20] J. Smith, L. Guttman, Trans. Metall. Soc. AIME 197 (1953) 81.
[21] J.W. Cahn, J.E. Hilliard, Trans. Metall. Soc. AIME 215 (1959) 759.
[22] S.J. Ford, J.-H. Hwang, J.D. Shane, R.A. Olson, G.M. Moss, H.M. Jennings, T.O. Mason, Adv. Cem. Bas. Mat. 5 (1997) 41.
[23] D.S. McLachlan, M.B. Blaszkiewicz, R.E. Newnham, J. Am. Ceram. Soc. 73 (1990) 2187.